International Journal of Global Research Innovations & Technology (IJGRIT)
e-ISSN : 2583-8717, Impact Factor: (Cosmos: 6.972 & I2OR: 5.002), Volume 04, No. 01, January-March, 2026, pp 82-92

Study of Stable and Efficient Photoelectrode for Photo-Electrochemical Splitting of Water

Hariom Jaimini[1*] | Lal Chand Yadav[2] | R.C. Meena[3] | S.L. Meena[4]

[1,2,3,4]Department of Chemistry, Jai Narain Vyas University, Jodhpur, Rajasthan, India.

*Corresponding Author: jaimini.hariom@gmail.com

Citation: Jaimini, H., Yadav, L., Meena, R.C. & Meena, S.L. (2026). Study of Stable and Efficient Photoelectrode for Photo-Electrochemical Splitting of Water. International Journal of Global Research Innovations & Technology, 04(01), 82–92.

ABSTRACT

One method that shows promise for producing hydrogen more easily and sustainably is photoelectrochemical (PEC) water splitting. PEC-based hydrogen generation solves the issue of solar persistency and offers a sustainable and environmentally friendly energy source. Despite significant attempts over the past few decades, no solar water splitting material has yet to meet the requirements of high efficiency, long-term stability, and affordability. The photoelectrode materials used in PEC must have band edge potentials at the surfaces, long-term stability against corrosion in the aqueous electrolyte, and enough voltage upon irradiation to split water. The oxygen and hydrogen evolution reaction are required for the charge transfer from the semiconductor's surface to the electrolyte. The most promising semiconductor materials are photocatalysts like TiO_2, WO_3, Fe_2O_3, Cu_2O, etc., because of their appropriate band gap and valance band structure. However, charge separation and conveyance are the main issues with PEC water splitting. The efficiency of the PEC process is increased by a number of techniques, including morphological control, defect introduction, heterojunction construction, and co-catalyst loading. The energy gap of n-type cuprous oxide (Cu_2O), which absorbs visible light up to a wavelength of 600 nm, makes it a suitable material for photocatalysis. Cu_2O's thickness is important as a photoelectrode since an incorrect thickness could deteriorate its photocatalytic qualities. By adjusting the Cu2O thickness, this work sought to improve the photocatalytic capabilities of Cu_2O electrodeposited on fluorine-doped tin oxide (FTO), or Cu_2O/FTO. Cu_2O/FTO electrochemical deposition allowed for the control of Cu_2O thickness by varying the deposition duration. Cu_2O's morphology altered from a leaf-like shape to an irregular facet shape with highly dense coverage when the deposition duration was varied from 8 to 40 minutes. The average thickness also rose from 450 to 1050 nm. Cu_2O/FTO achieved the highest photocurrent (150 and 158 μA under irradiation of 450 and 570 nm, respectively) at a thickness of 900 nm because of its extremely dense morphology and high absorption. Additionally, the charge diffusion was still good at a thickness of 900 nm. Further, the increase of Cu_2O film thickness higher than 900 nm caused low photocatalytic properties even though the morphology was highly dense, and the absorption was the highest. This state might result from Cu_2O's comparatively too high resistance, which led to inadequate charge dispersion.

***Keywords**: Hydrogen Generation, Photoelectrodes, Photocatalysts, PEC Water Splitting.*

Introduction

One ideal way to store renewable energy is to split water using photoelectrochemical (PEC) processes to convert solar energy into hydrogen. The most environmentally benign method of directly converting solar energy into chemical energy with no carbon emissions is the creation of hydrogen [1]. Due to their electrical and photocatalytic qualities for PEC water splitting, semiconductor materials have garnered a lot of interest in the last ten years. Water splitting produces hydrogen fuel, which is a sustainable and environmentally friendly energy source [2].

As an energy carrier, hydrogen can store enormous amounts of energy that can be used in a variety of sectors, including transportation, power generation, and the chemical industry. However, the natural gas reforming process is currently the most widely used method for producing hydrogen the reliance on fossil fuels for hydrogen, a number of researchers are attempting to create innovative devices using renewable energy sources.

In contrast to photovoltaic combined with electrolysis (PV-E) and photocatalysis (PC), photoelectrochemical (PEC) water splitting is a prominent method of producing hydrogen by solar water splitting. The hydrogen evolution reaction (HER) and oxygen evolution reaction (OER) in PEC take place at easily separable electrodes and offer a practical way to produce hydrogen. Both n-type and p-type semiconductor materials are used by PEC to create photoelectrodes. In order to drive the OER, electrons are gathered in the photoanode and subsequently transferred to the counter electrode when an n-type photoelectrode is utilized. In contrast, HER occurs at the semiconductor/liquid interface in a p-type semiconductor photocathode by sending electrons in the direction of the electrolyte. The reliance on fossil fuels for hydrogen, a number of researchers are attempting to create innovative devices using renewable energy sources.

In 1972, Fujishima and Honda [3] described the process of PEC water splitting to generate hydrogen using a TiO_2 photocatalyst. Many n-type (ZnO, TiO_2, Fe_2O_3) and p-type (NiO, Cu_2O) semiconductor materials have since been described for PEC water splitting systems. Because of their broad band gap structure, semiconductor materials like $SrTiO_3$, WO_3, and SnO_2 are stable in aqueous electrolyte but show low photocatalytic activity. Several modification techniques, such as doping, bilayered systems, and nanostructured creation, have been used to achieve the desired qualities in order to overcome the shortcomings in all kinds of semiconductor materials [4]. Over the past few decades, significant efforts have been undertaken to attain desired qualities in semiconductor material that simultaneously satisfy the PEC water splitting system's requirements for high efficiency, long-term stability, and low cost.

Because PEC uses solar energy to create hydrogen gas (H_2) through PEC water splitting [8] and to reduce water pollution through photocatalytic degradation of contaminants [9], the topic of PEC research is highly sought after. Cuprous oxide (Cu_2O) has a low energy gap (2.0–2.6 eV), making it a suitable material for PEC that functions under visible light irradiation [11, 12]. The redox potentials of water align with the edge locations of Cu_2O 's valence band (VB) and conduction band (CB). In comparison to the oxidation potential of H_2O to O_2 (0.62 vs. Ag/AgCl), the VB of Cu_2O (0.65 vs. Ag/AgCl) is at a greater positive potential at pH 7, but the CB of Cu_2O (−1.35 vs. Ag/AgCl) is at a more negative potential than the reduction potential of H^+ to H2 (−0.62 vs. Ag/AgCl) [12].

Cu_2O photocatalysis is also quite common due to its low cost, abundance in nature, and non-toxicity [13]. Due to copper vacancies in the crystal structure, Cu_2O is often a p-type semiconductor [14, 15]. For photocatalytic reduction processes, the p-type Cu_2O serves as a photocathode [15, 16]. Cu_2O, an n-type semiconductor created by oxygen vacancies, is currently being manufactured by several researchers [17–19]. For photocatalytic oxidation processes, n-type Cu_2O serves as a photoanode [18, 19].

Many techniques, including sputtering [20], thermal oxidation [21], chemical immersion [22], electrochemical deposition [23], and others, can be used to create Cu_2O. Because it is inexpensive, highly scalable, and simple to use, electrochemical deposition is the most widely used thin film deposition technique for producing Cu_2O. By varying electrochemical deposition parameters including voltage, duration, and solution pH, this technique may alter conductivity type, morphology, facets, and thickness [14]. For instance, Cu_2O photoelectrodes made at pH 6.5 had n-type conductivity, but those made at pH 11 demonstrated p-type conductivity [24]. Additionally, the shape and thickness of n-type Cu_2O may be altered by varying the deposition time [25].

By altering the electrochemical deposition method's deposition parameters, several studies have tried to improve the photocatalytic performance of n-type Cu_2O [17–19, 26]. Cu_2O film thickness as a photoelectrode can influence both photon absorption and charge diffusion; an increase in film thickness can enhance light absorption while decreasing charge diffusion [27]. Therefore, maximizing the photocatalytic activity of n-type Cu_2O requires optimizing the Cu_2O film thickness. Nevertheless, no research has been done on the ideal film thickness of n-type Cu_2O to improve its photocatalytic qualities.

In order to improve the photocatalytic capabilities of n-type Cu_2O placed on fluorine-doped tin oxide (FTO) using the electrochemical deposition technique, this work sought to determine the threshold

thickness of n-type Cu_2O.Research is going on in search of new materials and the improvement of existing low cost photoelectrodes. Therefore, a new bench- mark photocatalysts is needed.

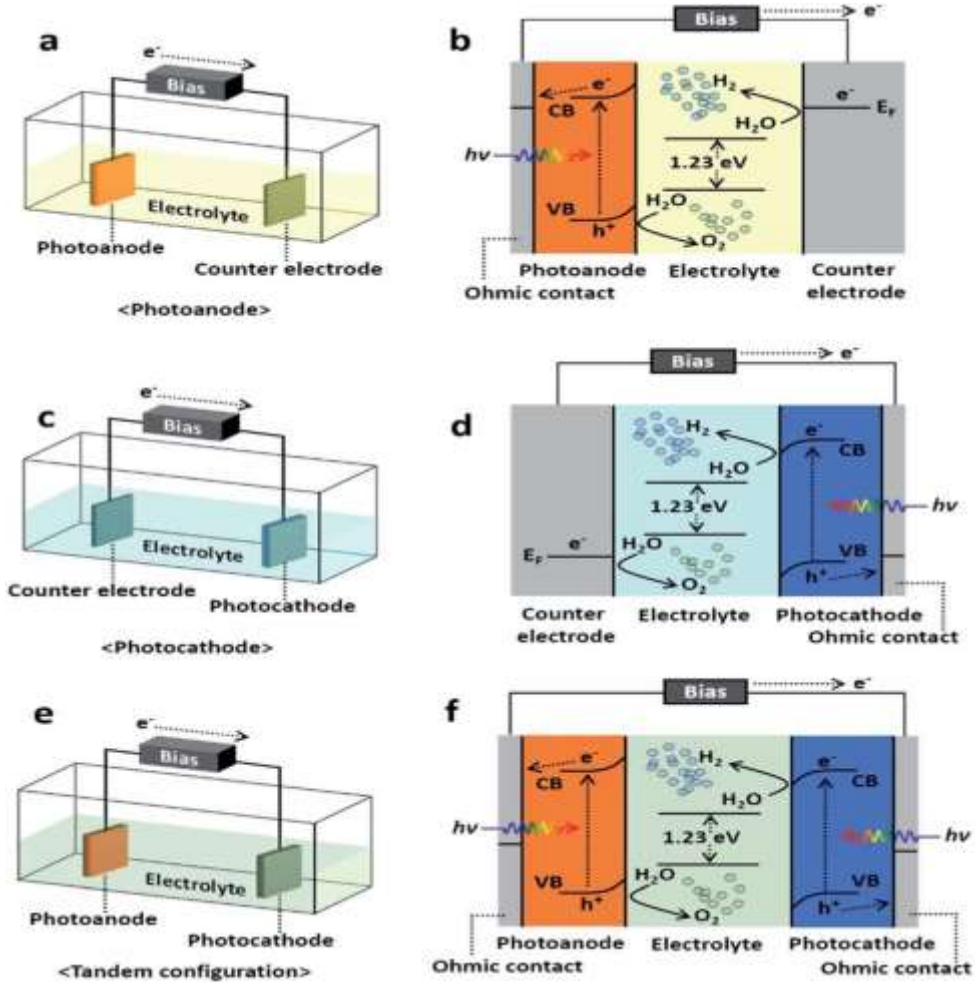

Fig. 1: A schematic diagram of PEC water splitting process [5]

Principle of PEC Water Splitting

In a PEC cell, a substrate as a thin film deposited on the photocatalyst to synthesize a photoelectrode that convert solar energy into electrical energy by using semiconductor/ electrolyte junction. Fig. 1 showed the process of photocatalytic water splitting achieved in a PEC used for conducting the reaction. The PEC method has principally involved 4 reaction steps:

- Generation of e^-/h^+ pairs on photoanode by light irradiation,
- Oxidation of water through e^-/h^+ pairs on the photo- anode to form O_2 and H^+,
- Transfer of e^- to cathode via an external circuit, and
- Reduction of H^+ on the cathode surface to produce H_2.

PEC cells typically have the benefit of less severe process, as there is no need for additional film deposition or coating equipment. Further, PEC system is also containing of high surface area photoanode for photocatalytic reaction.

In addition, several photoanode materials that can readily achieve an internal bias must be synthesized for PEC systems. This bias increases the photocatalytic activity for the PEC process by encouraging the separation of the e–/h+ (electron/hole pair). In order to further distinguish between the

electrodes, internal and external bias have also been required. Therefore, if the open circuit potential in a water-splitting system is less than 1.23 V, an external bias might be needed to raise the electrodes' reduction potential, which would speed up movement and finish the process.

PEC conditions to decompose water in H_2 and O_2, is widely regarded as the dawn of artificial photosynthesis work as per the following reaction mentioned below [6].

$2H^+ + 2e^- \rightarrow H_2$ (g) (1)

(HER: H_2 evolution reaction)

$2H_2O \rightarrow O_2 + 4H^+ + 4e^-$ (2)

(OER: O_2 evolution reaction)

Overall: $2H_2O \rightarrow O_2 + 2H_2$ (3) (light condition)

($\Delta E^o = -1.23$ V)

($\Delta G^o = 237.18$ kJ·mol^{-1})

The negative value of the standard electrodynamic potential means that the splitting of water is thermodynamically uphill, and the reaction requires additional energy. Relative to HER (which requires 2 electrons and 2 protons), OER is much more complex since 4 electrons and 4 protons are needed.

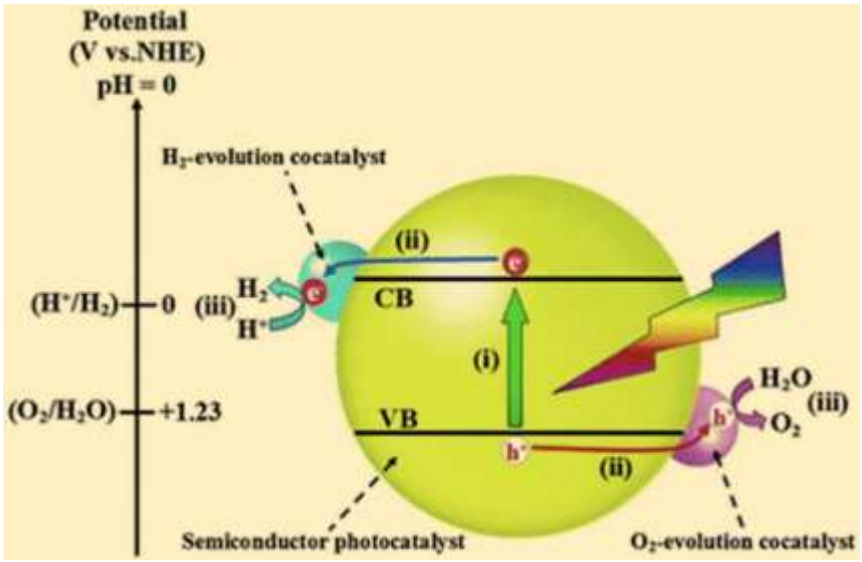

Fig. 2: Schematic description of band gap [7]

Basics to select a Photoelectrodes Material for PEC

There are various considerations for selecting a semi- conductor as a photoelectrode.

- **Potential Requirement**

Under normal circumstances, the water splitting reaction can only occur if the potential difference between the two half reactions is more than 1.23 eV (ΔG^o = 237.1 kJ mol–1), meaning that the average bandgap of the semiconductor must be greater than 1.23 eV. It is necessary to include additional energy losses, particularly the overpotential loss at the electrodes and the loss of ionic conductivity in the electrolyte. In a working cell, the actual potential demand typically exceeds 1.6 V.

- **Suitable Band Structure**

Along with an adequate bandgap, appropriate conduction and valance band edge positions should be considered for water reduction and oxidation reactions, respectively. Because of factors like solvent adsorption, values from conventional vacuum-based experiments are frequently unreliable. Instruments like ultraviolet photoelectron spectroscopy (UPS), which reports on the ionizing energy (basically the valence band maximum energy, eV), frequently require experimental observations to determine the relative positions of the band boundaries.

- **Elevated Surface Area and Crystallization**

For effective charging separation and processing, semiconductors with high surface activity for the OER/HER reactions and high crystallinity for charge transports are needed.

- **Stability**

When using splitting solar water, stability is crucial. In electrolytes with a specific pH range, the photoelectrode need to be stable. To extend their lifespan, the photoelectrodes could require efficient shielding. This function requires a protective covering that is optically transparent and does not interfere with the photoelectrode's ability to absorb light.

- **Low Cost**

The system's economic cost is one of the most important factors in PEC. For widespread use, we require materials made of elements that are abundant on Earth. Cu_2O and hematite (a-Fe_2O_3) are good examples of it. Due to their stability, appropriate band gap, and activity for hydrogen evolution rate (HER) under solar irradiation, numerous semiconductor materials have been the subject of intriguing research in recent years.

Solar-to-Hydrogen Conversion Efficiency (STH Efficiencies)

Efficiency of solar-to-hydrogen (STH) is a measure of the conversion of the generated H_2 from incident solar energy to the chemical energy. If the photogenerated carriers are in- volved in the division of energy, and the products are stoichiometric (H_2:O_2 = 2:1), then STH efficiencies under one-sun irradiation can be represented as:

$$\mathrm{STH} = \frac{((\mathrm{mmol\ H_2S^{-1}})\times(273\ \mathrm{kJ\ mol^{-1}}))}{P\ (\mathrm{mW\ cm^{-2}})\times\mathrm{Area}\ (\mathrm{cm^2})} \quad (4)$$

where, mmol H_2/s is the rate of H_2 production and the Gibbs free energy of H_2 is 237 kJ·mol^{-1}. H_2 production rate can be found by mass spectrometry or gas chromatography. If we know the current, voltage, and the faradaic efficiency (η_F), eq. (4) may be modified as:

$$\mathrm{STH} = \frac{(|J_{SC}\ (\mathrm{mA.\ cm^{-2}})|\times 1.23\ \mathrm{V}\times(\eta_F)}{(P\ (\mathrm{mW.\ cm^{-2}}))} \quad (5)$$

The faradaic efficiency for HER and OER is supposed to be 100%. Then, eq. (5) could be represented as:

$$\mathrm{STH} = \frac{1.23\ \mathrm{V}\times J_{SC}}{P_{IN}} \quad (6)$$

where J_{SC} is a short circuit current density and P_{IN} is the overall photon energy flux input into the cell (i.e. for simulated solar light AM 1.5 G, 100 mW·cm^{-2}). The STH efficiencies can be achieved in a configuration with two electrodes (determination from a test with three electrodes also leads to miscalculations).

Materials and Methods

- **Preparation of Cu2O/FTO**

An electrochemical process was used to create Cu_2O layer in a three-electrode cell via electrochemical deposition [19]. FTO served as the working electrode, Ag/AgCl served as the reference electrode, and a Pt plate served as the counter electrode. A mixed solution of 0.02 M $Cu(CH_3COO)_2$ served as the electrolyte for the electrodeposition of Cu_2O /FTO. 40 mL of deionized (DI) water containing 0.1 M $NaCH_3COO$ (Powder, 99%, Sigma-Aldrich) and H_2O. Using 0.5 M CH_3COOH (Renkem chemical), the electrolyte's pH was brought to 6.5. Since every chemical was in good purity, repurification was not necessary. Prior to the start of deposition, the FTO was cleaned in an ultrasonic cleaner for ten minutes each using a solution of acetone, ethanol, and DI water.

The electrochemical deposition was then performed under various deposition durations (8, 16, 24, 32 and 40 min) at a voltage of −0.2 V vs. Ag/AgCl. The electrolyte temperature was maintained at 65 °C throughout the deposition procedure. The as-prepared sample, known as Cu_2O/FTO, was then cleaned with DI water and dried for around five minutes using nitrogen gas.

In order to quantify thickness, Cu_2O /FTO was also manufactured with a "step height" on its surface. The sample was prepared using the same method as the original Cu_2O /FTO. Nevertheless, prior to the electrodeposition procedure, the FTO was altered. A tape measuring 0.5 cm by 1 cm was affixed to the centre of the FTO surface.

The electrochemical deposition was then performed under various deposition durations (8, 16, 24, 32 and 40 min) at an electrolyte temperature of 65°C and a voltage of −0.2 V vs. Ag/AgCl. After completion, the tape was removed from the FTO surface. Following that, DI water was used to wash the as-prepared Cu_2O /FTO with a "step height," and nitrogen gas was used to dry it for about five minutes.

- **Characterization of Cu2O/FTO**

Several methods were used to characterize Cu_2O /FTO. Prior to the characterization, the Cu_2O /FTO was cleaned of dust by purging it with nitrogen gas for about five minutes. Atomic Force Microscopy (AFM) was used to view the topography of Cu_2O. AFM was used to measure the thickness of Cu_2O. The Cu_2O /FTO was manufactured as a step height sample for this measurement. X-ray diffractometry (XRD) was used to record the crystal structure at an incidence wavelength of 1.54 Å.

Raman spectroscopy was used to detect the vibration modes using an excitation wavelength of 532 nm (2.1 $mW.\mu m^{-2}$). Ultraviolet–visible (UV–vis) spectroscopy using an integration sphere and a Xe lamp was used to measure the light absorption spectra.

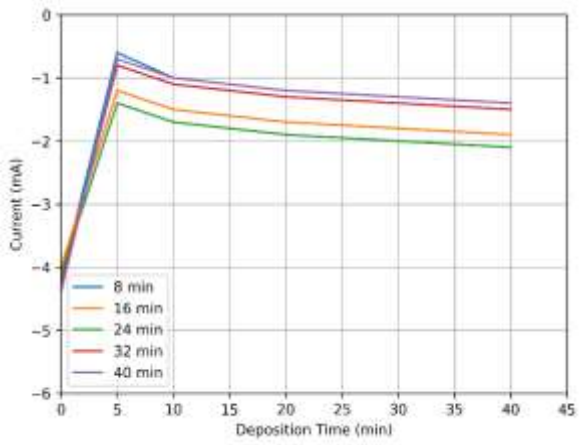

Figure 3: Current of Cu2O/FTO Recorded during Electrochemical Deposition process under Different Deposition Times

Results and Discussion

- **Effect of Deposition Time on Morphology, Thickness, and Properties of Cu2O/FTO**

Using an electrochemical deposition technique, Cu_2O/FTO was created by applying a constant voltage (−0.2 V vs. Ag/AgCl) during a range of deposition durations (8–40 min). The reaction of

$$2Cu^{2+} + 2OH^- + 2e^- \rightarrow Cu_2O + H_2O$$

led to the production of Cu_2O on the FTO substrate in the solution containing $Cu(CH_3COO)_2$ [29]. As shown in Figure 3, the current that resulted from the deposition procedure was recorded against the deposition time. The Cu_2O nucleation-growth process, which has three areas, was clearly visible in the deposition current [30, 31].

Due to the conductive FTO with a sheet resistance of 22 Ω/sq, the first current region first demonstrated that the Cu_2O growth process started with the nucleation of Cu_2O grains on the FTO surface, which was characterized by a strong cathodic current rapidly approximately 30 s [19]. The cathodic current rose quickly, suggesting that surface diffusion of Cu^{2+} with uniform input flux regulated the rate of Cu_2O deposition [32, 33]. Following that, the number of Cu_2O grains grew and covered the FTO surface as time rose. This resulted in a larger resistance on the FTO surface, as seen by the

cathodic current decreasing until it reached its maximum before dying. Each Cu_2O grain formed in the diffusion zone under these circumstances. The cathodic current decreased to equilibrium and additional Cu_2O material developed on the FTO surface in the third current area. Ultimately, the whole surface of FTO was coated in Cu_2O material. The shape and roughness of Cu_2O on the FTO surface may be regulated by surface diffusion [33]. The total charge (electric current times deposition time) during the electrochemical deposition process dictated the grain number, and the amount of Cu_2O material on the FTO surface was dependent on the deposition timings. As a result, the Cu_2O film thickness rose as the deposition period increased due to an increase in the number of Cu_2O grains [18]. AFM was used to observe the Cu_2O/FTO topography, which is shown in Figure 2. The deposition period affected the Cu_2O's morphology on the FTO substrate. The shape of the deposition current matched the alteration in Cu_2O morphology. Cu_2O deposited for 8 minutes produced three leaf-like grains with 500–800 nm-long dendritic branches, as seen in Figure 4(a). Because the surface diffusion of Cu_{2+} in the plating solution was unable to replenish the deposition, the Cu_2O grains produced on the FTO surface displayed branching dendritic development [8]. Other investigations have also noted that Cu_2O grains have a leaf-like morphology [31, 34].

As demonstrated in Cu_2O deposited for 16 minutes (Figure 4(b)) and 24 minutes (Figure 4(c)), Cu_2O branches developed vertically, producing a thicker Cu_2O film that covered the leaf-like form of Cu_2O grains. The Cu_2O surface displayed a porous topology under these circumstances. After 32 minutes (Figure 4(d)) and 40 minutes (Figure 4(e)) of deposition, the leaf-like shape of Cu_2O was no longer discernible. The nonuniform distribution of Cu^{2+} during the electrodeposition may have contributed to the Cu_2O surface's uneven faceted shape and very dense coverage in this instance.

The surface area and roughness also changed with the deposition period, according to the topography picture analysis.

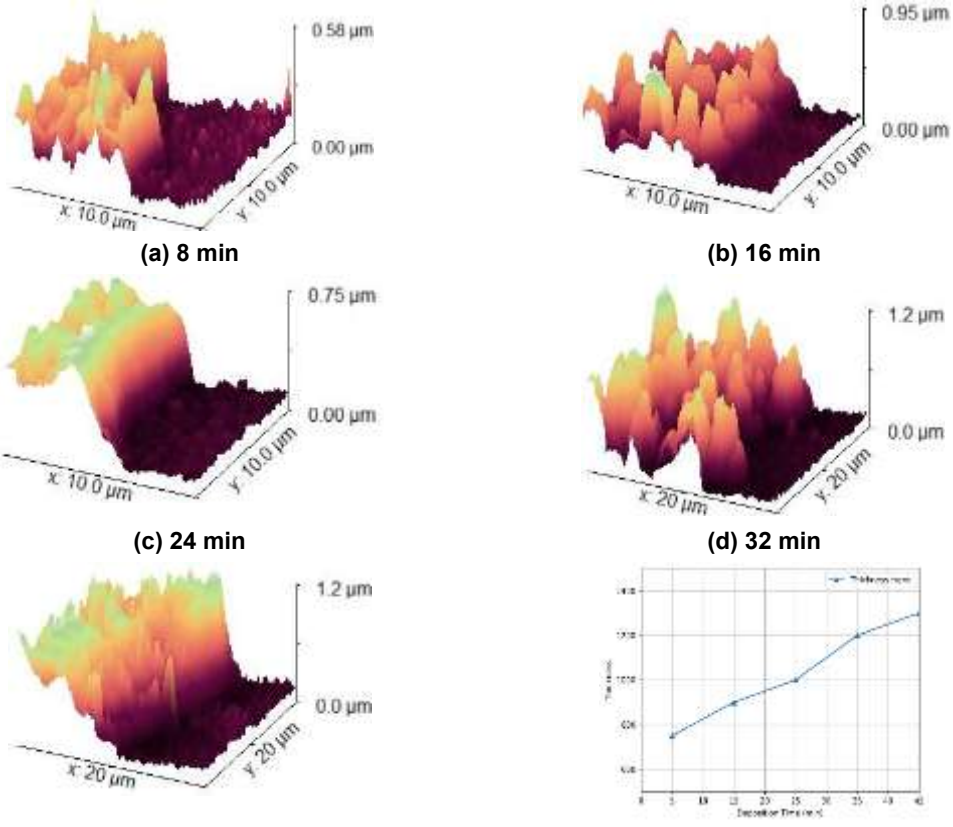

(a) 8 min **(b) 16 min**

(c) 24 min **(d) 32 min**

(e) 40 min **(f)**

Figure 4: 3D AFM images showing thicknesses of Cu_2O on FTO substrate deposited under different deposition times.

Under the deposition times of 8, 16, 24, 32, and 40 min, the rough nesses of Cu_2O were 151.5, 133.5, 220.7, 122.8, and 159.2 nm, respectively. Meanwhile, the surface areas were 130.3, 123.9, 133.5, 115.7, and 123.7 μm^2. The surface diffusion of Cu^{2+} in the electrodeposition, in addition to the substrate conductivity, was responsible for the changes in morphology, roughness, and surface area with the deposition time [33].

AFM was used to measure the Cu_2O thickness on the FTO substrate. However, it was challenging to observe the "step height" using the camera (CCD) in the AFM system because Cu_2O was not reflective enough. In order to make the boundaries between FTO and Cu_2O visible due to the reflecting Au/glass, the Cu_2O/FTO with a "step height" was positioned on top of the Au/glass. The AFM cantilever was then precisely positioned on the Cu_2O/FTO border by adjusting its location.

A "step height" profile was then created by performing AFM scanning horizontally, Along with improved Cu_2O grain density and coverage on the FTO surface, the Cu_2O film thickness grew from 450 to 1050 nm as the deposition period increased [25,35]. This outcome was in line with the rise in total charge that occurred during electrochemical deposition.

To determine if Cu_2O was present on the FTO surface, XRD and Raman scattering measurements were used. The XRD patterns of Cu_2O/FTO deposited throughout a range of deposition durations, from 5 to 45 minutes, are displayed in Figure 4(a). The (111), (200), and (220) crystal planes of pure Cu_2O (ICSD No. 98 -006-0719) were represented by several peaks in the XRD patterns with 2θ values of 36.58, 42.29, and 61.30°, respectively [10, 14].

Cu_2O grew preferentially along the (111) direction, as evidenced by the (111) peak's greater intensity compared to peaks indexed to (200) and (220). As demonstrated by the Cu_2O/FTO deposition duration of 8 to 24 minutes, the strength of the (111) and (200) peaks varied with deposition time, with an increase in crystallinity in the (111) and (200) orientations. However, Cu_2O/FTO deposited for 32 and 40 minutes displayed a reduction in (111) and (200) orientations, which may be explained by Cu_2O/FTO's lack of leaf-like morphology. The FTO substrate (98-006-0719), respectively, is the source of another peak in the XRD pattern [10, 14].

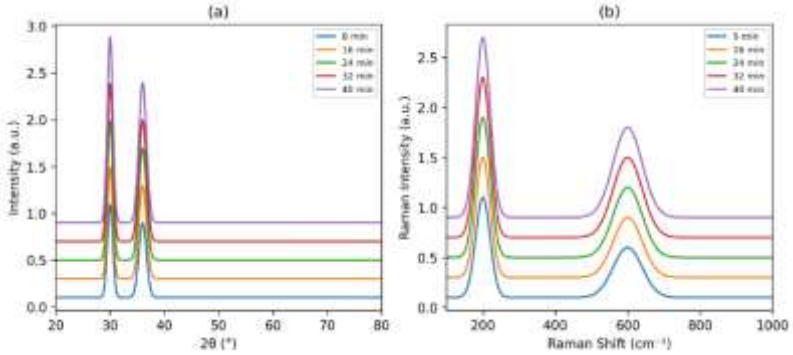

Figure 5: (a) XRD patterns and (b) Raman specta of Cu2O/FTO deposited under different deposition times

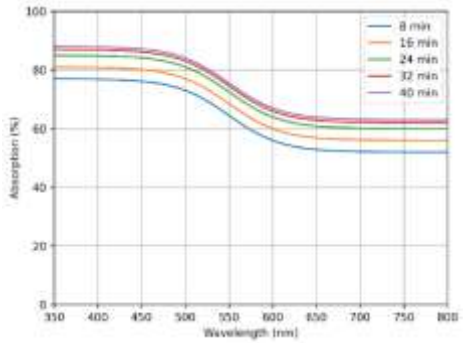

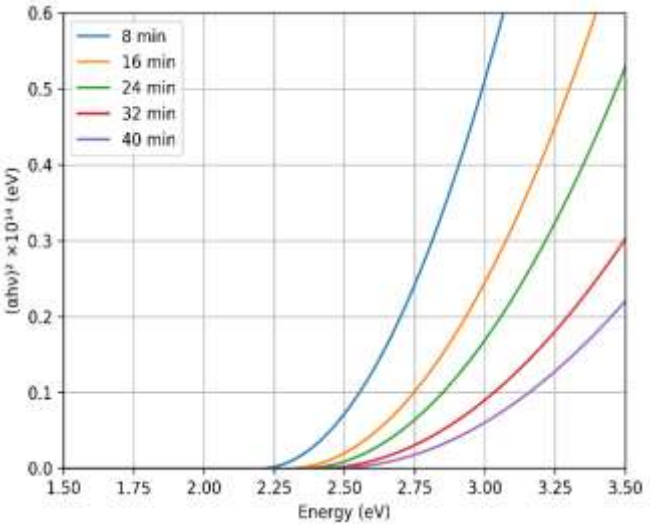

Figure 6: (a) Absorption spectra and (b) Tauc-plots of Cu2O/FTO deposited under different deposition times

Figure 6 (b) displays the Cu_2O /FTO's Raman spectra. The Raman spectrum of Cu_2O is represented by a number of peaks at Raman shifts of 146, 218.5, 413.7, 503.1, and 628.8 cm^{-1} [36].

The deposition periods did not significantly alter the Raman peaks. The successful electrodeposition of Cu_2O was validated by the Raman scattering spectra and XRD patterns. No further copper oxide phases were discovered; only Cu_2O was formed on the FTO surface.

UV–vis spectroscopy was used to capture the light absorption spectra of Cu2O/FTO. As seen in Figure 6(a), Cu_2O /FTO demonstrated strong light absorption in the 350–600 nm spectral range, which is consistent with earlier research [11, 31, 37]. As the deposition duration grew, so did the light absorption. It showed that the amount of Cu_2O materials on the FTO substrate due to the longer deposition time was related to the greater Cu_2O thickness, which produced the higher light absorption.

With a higher thickness, the distribution of the intensity of the radiant energy inside the Cu2O was also higher [27]. As the deposition durations increased, a red change at the absorption edge was seen, which is consistent with the Cu_2O color shifting from yellow to reddish. Light scattering losses during the experiment were the source of the apparent absorption seen at wavelengths longer than 600 nm. Cu_2O /FTO had bandgap energies of 2.4, 2.3, 2.2, 2.1, and 2.0 eV for deposition times of 8, 16, 24, 32, and 40 minutes, respectively, according to tauc-plots of the material, which were computed from the absorption coefficient assuming a direct band gap, $(\alpha h\nu)^2$ (Figure 6(b)). Cu_2O has a band gap energy of around 2 eV, which allows it to absorb solar visible light [11, 15]. The wavelength of light that may be absorbed increases with the deposition time.

Conclusion

Investigations were conducted into the photocatalytic characteristics of n-type Cu_2O at various Cu_2O thicknesses. Electrochemical deposition was used to place the Cu_2O on an FTO substrate. By varying the deposition duration from 5 to 45 minutes, the Cu_2O film thickness was managed. AFM, XRD, Raman spectroscopy, and UV–vis spectroscopy was among the methods used to assess the Cu_2O/FTO's quality. The morphological shape of the Cu_2O was dependent on the duration of deposition; as the duration of deposition increased, the Cu_2O coverage became denser. As the deposition period rose, the Cu_2O thickness also increased. Light up to 600 nm in wavelength (band gap energy of 2.0 eV) may be absorbed by the Cu_2O/FTO. Due to the rise in film thickness, the Cu_2O/FTO absorption increased as the deposition time rose.

By monitoring the photocurrent under UV and visible light irradiation, the photocatalytic characteristics of the Cu_2O/FTO were examined. With a threshold thickness of around 1000 nm, the Cu_2O /FTO showed anodic photocurrent behavior and tended to grow with increasing deposition time before decreasing after 32 minutes. The Cu_2O/FTO showed the maximum anodic photocurrent at a thickness of 900 nm, which was explained by its ideal thickness for light absorption, extremely dense

Cu_2O coverage, and rather good charge diffusion. No increase in photocurrent was seen when Cu_2O thickness was further increased. Even though the morphology displayed extremely dense coverage and the absorption was strong, the photocatalytic capabilities of the Cu_2O/FTO deposited at 40 minutes were the lowest. This was due to the comparatively high resistance of Cu_2O, which led to poor charge diffusion.

The PEC water splitting technique to create hydrogen has some challenges, including poor absorption in the visible spectrum, low durability photo corrosion, and sluggish surface dynamics. There is a lot of study being done to close the gap. This study provides a short description of the fundamental idea of PEC, its mechanism, and the present state of photoelectrode and electrocatalysts. In addition, the qualities needed in the PEC process were investigated, as well as the appropriate electrode material.

References

1. Pan, L., Liu, Y., Yao, L., Ren, D., Sivula, K., Grätzel, M., & Hagfeldt, A. (2020). Title not provided. Nature Communications, 11, 1.
2. Tabish, A., Varghese, A. M., Wahab, M. A., & Karanikolos, G. N. (2020). Title not provided. Catalysts, 10, 95. https://doi.org/10.3390/catal10010095
3. Fujishima, A., & Honda, K. (1972). Electrochemical photolysis of water at a semiconductor electrode. Nature, 238, 37–38.
4. Salomão, P. E. A., Barbosa, L. R. S., Andrade, T. S., Ferreira, E. J. C., & Pereira, M. C. (2019). Title not provided. International Journal of Hydrogen Energy, 54, 28603.
5. Bhatt, M. D., & Lee, J. S. (2015). Title not provided. Journal of Materials Chemistry A, 3, 10632.
6. Grätzel, M. (1981). Title not provided. Accounts of Chemical Research, 14, 376.
7. Yang, L., Zhou, H., Fan, T., & Zhang, D. (2020). Title not provided. Physical Chemistry Chemical Physics. https://doi.org/10.1039/C4CP00246F
8. Lin, L., Hisatomi, T., Chen, S., Takata, T., & Domen, K. (2020). Visible-light-driven photocatalytic water splitting: Recent progress and challenges. Trends in Chemistry, 2, 813–824. https://doi.org/10.1016/j.trechm.2020.06.006
9. Nazim, M., Khan, A. A. P., Asiri, A. M., & Kim, J. H. (2021). Exploring rapid photocatalytic degradation of organic pollutants with porous CuO nanosheets. ACS Omega, 6, 2601–2612. https://doi.org/10.1021/acsomega.0c04747
10. Khasanah, R. A. N., Lin, H.-C., Ho, H.-Y., Peng, Y.-P., Lim, T.-S., Hsiao, H.-L., Wang, C.-R., Chuang, M.-C., & Chien, F. S.-S. (2021). Substrate-dependent photocatalytic properties of Cu_2O heterojunctions. RSC Advances, 11, 4935–4941. https://doi.org/10.1039/D0RA10681J
11. Laidoudi, S., Bioud, A. Y., Azizi, A., Schmerber, G., Bartringer, J., Barre, S., & Dinia, A. (2013). Growth and characterization of electrodeposited Cu_2O thin films. Semiconductor Science and Technology, 28, 115005. https://doi.org/10.1088/0268-1242/28/11/115005
12. Khasanah, R. A. N., Lin, H.-C., Ho, H.-Y., Peng, Y.-P., Hsiao, H.-L., Wang, C.-R., & Chien, F. S.-S. (2022). Photoelectrocatalytic hydrolysis of ammonia borane by electrodeposited Cu_2O. International Journal of Hydrogen Energy, 47, 11203–11210. https://doi.org/10.1016/j.ijhydene.2022.01.167
13. Koiki, B. A., & Arotiba, O. A. (2020). Cu_2O as an emerging semiconductor in photocatalysis: A review. RSC Advances, 10, 36514–36525. https://doi.org/10.1039/D0RA06858F
14. Hossain, M. A., Al-Gaashani, R., Hamoudi, H., Al Marri, M. J., Hussein, I. A., Belaidi, A., Merzougui, B. A., Alharbi, F. H., & Tabet, N. (2017). Controlled growth of Cu_2O thin films by electrodeposition. Materials Science in Semiconductor Processing, 63, 203–211. https://doi.org/10.1016/j.mssp.2017.02.012
15. Bagal, I. V., Chodankar, N. R., Hassan, M. A., Waseem, A., Johar, M. A., Kim, D.-H., & Ryu, S.-W. (2019). Cu_2O as an emerging photocathode. International Journal of Hydrogen Energy, 44, 21351–21378. https://doi.org/10.1016/j.ijhydene.2019.06.184
16. Son, M.-K. (2021). Large-scale Cu_2O photocathodes design. Energies, 14, 7422. https://doi.org/10.3390/en14217422
17. McShane, C. M., & Choi, K.-S. (2009). Photocurrent enhancement of Cu_2O electrodes. Journal of the American Chemical Society, 131, 2561–2569. https://doi.org/10.1021/ja806370s

18. Chen, Y.-C., Chen, Y.-J., Dong, P.-H., & Hsu, Y.-K. (2020). Photoelectrochemical water splitting by Cu_2O. ACS Applied Energy Materials, 3, 1373–1380. https://doi.org/10.1021/acsaem.9b01781
19. Khasanah, R. A. N., Lee, C.-H., Li, Y. C., Chen, C.-H., Lim, T.-S., Wang, C.-R., Chang, P.-Y., Sheu, H.-S., & Chien, F. S.-S. (2022). Enhancement of photocatalytic activity of Cu_2O. ACS Applied Energy Materials, 5, 15326–15332. https://doi.org/10.1021/acsaem.2c02963
20. Dolai, S., Das, S., Hussain, S., Bhar, R., & Pal, A. K. (2017). Cu_2O thin films by sputtering. Vacuum, 141, 296–306. https://doi.org/10.1016/j.vacuum.2017.04.033
21. Karapetyan, A., Reymers, A., Giorgio, S., Fauquet, C., Sajti, L., Nitsche, S., Nersesyan, M., Gevorgyan, V., & Marine, W. (2015). Cu_2O thin films by thermal oxidation. Journal of Luminescence, 159, 325–332. https://doi.org/10.1016/j.jlumin.2014.10.058
22. Saadaldin, N., Alsloum, M. N., & Hussain, N. (2015). Copper oxides thin films by CBD. Energy Procedia, 74, 1459–1465. https://doi.org/10.1016/j.egypro.2015.07.794
23. Abdelfatah, M., Ledig, J., El-Shaer, A., Sharafeev, A., Lemmens, P., Mosaad, M. M., Waag, A., & Bakin, A. (2016). Electrodeposition modes effect on Cu_2O solar cells. ECS Journal of Solid State Science and Technology, 5, Q183–Q187. https://doi.org/10.1149/2.0191606jss
24. Rahal, H., Kihal, R., Affoune, A. M., & Rahal, S. (2020). Effect of pH on Cu_2O thin films. Journal of Electronic Materials, 49, 4385–4391. https://doi.org/10.1007/s11664-020-08093-y
25. Mohd Hanif, A. S., Azmal, S. A., Ahmad, M. K., & Mohamad, F. (2015). Effect of deposition time on Cu_2O films. Applied Mechanics and Materials, 773, 677–681. https://doi.org/10.4028/www.scientific.net/AMM.773-774.677
26. Kalubowila, K. D. R. N., Gunawardhana, L. K. A. D. D. S., Wijesundera, R. P., & Siripala, W. (2014). Improving photoconductivity of Cu_2O films. Semiconductor Science and Technology, 29, 075012. https://doi.org/10.1088/0268-1242/29/7/075012
27. Camera-Roda, G., & Santarelli, F. (2007). Optimization of photocatalytic film thickness. Catalysis Today, 129, 161–168. https://doi.org/10.1016/j.cattod.2007.06.062
28. Osorio-Aguilar, D. M., et al. (2023). Adsorption and photocatalytic degradation of methylene blue. Catalysts, 13, 1480. https://doi.org/10.3390/catal13121480
29. Qi, G., Liu, M., Tang, C., Chang, J., Yang, C., Liu, F., Ning, X., & Yang, Y. (2021). Conductivity control of Cu_2O films. International Journal of Hydrogen Energy, 46, 2878–2889. https://doi.org/10.1016/j.ijhydene.2020.04.176
30. Ait Hssi, A., et al. (2020). Optical properties of Cu_2O films. Materials Research Express, 7, 016424. https://doi.org/10.1088/2053-1591/ab6772
31. Yang, Y., Han, J., Ning, X., Cao, W., Xu, W., & Guo, L. (2014). Morphology control of Cu_2O films. ACS Applied Materials & Interfaces, 6, 22534–22543. https://doi.org/10.1021/am506657v
32. Yu, X., Tang, X., Li, J., Zhang, J., Kou, S., Zhao, J., & Yao, B. (2017). Nucleation of Cu_2O films. Journal of The Electrochemical Society, 164, D999–D1005. https://doi.org/10.1149/2.1081714jes
33. Brandt, I. S., et al. (2015). Substrate effects in Cu_2O electrodeposition. Journal of Applied Physics, 118, 145303. https://doi.org/10.1063/1.4932642
34. Wang, P., Wu, H., Tang, Y., Amal, R., & Ng, Y. H. (2015). Cu_2O photoelectrodes. Journal of Physical Chemistry C, 119, 26275–26282. https://doi.org/10.1021/acs.jpcc.5b07276
35. Taher, S. J., Barzinjy, A. A., & Hamad, S. M. (2020). Deposition time effect on Cu_2O nanocubes. Journal of Electronic Materials, 49, 7532–7540. https://doi.org/10.1007/s11664-020-08495-y
36. Benz, J., Hering, K. P., Kramm, B., Polity, A., Klar, P. J., Siah, S. C., & Buonassisi, T. (2017). Nitrogen doping in Cu_2O. Physica Status Solidi B, 254, 1600421. https://doi.org/10.1002/pssb.201600421
37. Chen, A., Long, H., Li, X., Li, Y., Yang, G., & Lu, P. (2009). Growth of Cu_2O and CuO films. Vacuum, 83, 927–930. https://doi.org/10.1016/j.vacuum.2008.10.003.

○○○